High-Throughput Automated Exploration of Phase Growth Behaviors in Quasi-2D Formamidinium Metal Halide Perovskites

Jonghee Yang,[1] Benjamin J. Lawrie,[2,3] Sergei V. Kalinin,[1] Mahshid Ahmadi[1]*

[1] *Institute for Advanced Materials and Manufacturing, Department of Materials Science and Engineering, University of Tennessee, Knoxville, TN 37996, United States*

[2] *The Center for Nanophase Materials Sciences, Oak Ridge National Laboratory, Oak Ridge, TN 37831, United States*

[3] *Materials Science and Technology Division, Oak Ridge National Laboratory, Oak Ridge, TN 37831, United States*

* E-mail: mahmadi3@utk.edu

Abstract

Quasi-two-dimensional (2D) metal halide perovskites (MHPs) are an emerging material platform for sustainable functional optoelectronics, however the uncontrollable, broad phase distribution remains a critical challenge for applications. This is because the basic principles for controlling phases in quasi-2D MHPs remain poorly understood, due to the rapid crystallization kinetics during the conventional thin-film fabrication process. Herein, a high-throughput automated synthesis-characterization-analysis workflow is implemented to accelerate material exploration in formamidinium (FA)-based quasi-2D MHP compositional space, revealing the early-stage phase growth behaviors fundamentally determining the phase distributions. Upon comprehensive exploration with varying synthesis conditions including 2D:3D composition ratios, antisolvent injection rates, and temperatures in automated synthesis-characterization platform, we observe that the prominent *n*=2 2D phase restricts the growth kinetics of 3D-like phases – α-$FAPbI_3$ MHPs with spacer-coordinated surface – across the MHP compositions. Thermal annealing is a critical step for proper phase growth, although it can lead to the emergence of unwanted local PbI_2 crystallites. Additionally, fundamental insights into the precursor chemistry associated with spacer-solvent interaction determining the quasi-2D MHP morphologies and microstructures are demonstrated. Our high-throughput study provides comprehensive insights into the fundamental principles in quasi-2D MHP phase control, enabling new control of the functionalities in complex materials systems for sustainable device applications.

Introduction

Metal halide perovskites (MHPs) have gained significant attention as materials for high-performance optoelectronic applications due to their favorable optoelectronic properties. The power conversion efficiency of photovoltaics (PVs) based on MHPs has reached up to ~25.8%[1] and green and red light-emitting devices (LEDs) based on MHPs have demonstrated emission efficiencies exceeding 20%.[2, 3] However, one of the major challenges hindering the widespread adoption of MHPs is their instability, which affects the long-term operation and durability of devices.[4, 5] Quasi-two-dimensional (2D) MHPs have recently garnered attention for their unique properties distinctive from those observed in three-dimensional (3D) MHP systems. Quasi-2D MHPs are represented by the chemical formula $L_2A_{n-1}B_nX_{3n+1}$, where L, A, B, and X represent the spacer cations confining the inorganic 2D lattices, monovalent organic/inorganic cations, divalent metal cations, and halides, respectively.[6-8]

Control over the thickness of the $[PbX_6]^{4-}$ octahedra unit in quasi-2D MHPs, denoted by *n*, manifests tunable bandgap and exciton binding energy in a quantum-well electronic structure, beneficial for LED applications.[3, 6, 9-13] Furthermore, quasi-2D MHPs offer improved phase stability compared to 3D MHPs due to the surface-protecting ability of spacer cations against external stresses. Particularly, the implementation of the quasi-2D structure into the long-range 3D MHP lattices that forms '3D-like phases' – a structure of 3D MHP lattice where the spacers are coordinated to the surface – leads to stability enhancement of MHP optoelectronics without compromising the band gap and performances.[13-15]

A major challenge in the development of quasi-2D MHP systems is the difficulty in obtaining a pure desired phase, as multiple phases are often formed during film fabrication.[16] Several efforts were attempted to regulate the multi-phase emergence via spacer engineering,[17] optimal 2D:3D MHP ratio,[13] and additive engineering.[3] Recently, the implementation of high-

throughput robotic synthesis platforms have opened a new avenue of materials explorations and processing optimizations,[18] not only accelerating the discovery of functional MHP compositions (particularly in 3D system) but also provides comprehensive insights into the phase distributions, physical properties and stability of the complex quasi-2D MHP systems.[19-21]

Nevertheless, all those strategies have exhibited limited success, which could be attributed to a lack in understanding of the phase growth behaviors of the complex quasi-2D MHP system. It has been shown that the broad phase distribution in quasi-2D MHP stems from the disproportionation of a kinetically-grown intermediate-*n* 2D phase.[17] Still, the understanding of early-stage formation and growth kinetics of quasi-2D MHP phases, primarily determining the phase distribution in the system before disproportionation, remains far elusive. The missing piece originates from the difficulty in capturing the features during the practical film fabrications such as spin-coating, which quickly takes place within a few seconds by solvent evaporation.

Herein, we systematically investigate the phase formation and growth kinetics of quasi-2D MHPs as a function of 2D:3D ratios via high-throughput synthesis and characterization of the microcrystals from the precursor solution, allowing for monitoring the early-stage phase evolution over time.[22, 23] Utilizing an integrated workflow based on high-throughput automated synthesis by pipetting robot, temporal photoluminescence (PL) characterization, and automated peak analysis, comprehensive phase growth kinetics in quasi-2D systems under different synthesis conditions – 2D:3D compositions, antisolvent injection rates and temperatures that are controlled in the automated platform – are explored.[22, 23] Formamidinium (FA) and phenethylammonium (PEA) cations are selected as building blocks for the 3D and 2D MHP systems, respectively, due to the excellent performances of the 3D FA MHP

optoelectronics,[1, 5] and it is well known that the incorporation of 2D PEA MHPs improves the stability of the entire system.[13] We note that the presented workflow in this study exploits an automated peak fitting function with a preset of rough information of PL characteristics for each phase in quasi-2D MHPs based on known physics, which is a stark difference from the previous experimental workflows. This enables more accurate assessment of the phase emergence features in the complex system.

We found that, unlike the broad phase distributions in methylammonium (MA)- or cesium (Cs)-based systems,[24] in the FA-based system, up to 95% of 3D $FAPbI_3$ ratio in a compositional space, the n=2 2D MHP is the most dominant and stable phase. Higher-n (n≥5) phases also develop alongside the n=2 phase with increasing the ratio of 3D MHP. However, the 3D-like MHPs only appear after the n=2 phase has been depleted (beyond 96% $FAPbI_3$ composition ratio). Note that these trends in the large quasi-2D compositional space are further confirmed by the unsupervised machine learning (ML) analysis of the PL spectra.

Characterizations of thin films further reveal that the emergence of the δ-$FAPbI_3$ phase – a room temperature stable non-perovskite phase – particularly at high 3D ratios[25, 26] inhibits the growth of 3D-like phases. Thermal annealing of the films converts the 2D phases to higher-n polymorphs, thereby leading to the appearance of 3D-like MHPs. Using hyperspectral cathodoluminescence (CL) microscopy, we reveal that thermal annealing results in formation of local PbI_2 crystallite byproduct, which may negatively impact the optoelectronic properties of the quasi-2D MHPs.[27] In addition, we found that the selection of solvent crucially impact on the surface morphologies, microstructures, and local phase inhomogeneities of the quasi-2D MHP films. Chemical principles associated with these features are proposed.

Our study exemplifies how a high-throughput synthesis platform can effectively accelerate our understanding of complex material systems with multiple functionalities. It provides

comprehensive insights into the phase growth kinetics of the quasi-2D MHPs and identifies crucial factors that should be considered when designing the formation mechanism of functional semiconductor systems.

Results and Discussion

High-throughput exploration of phase evolution kinetics in PEA-FA quasi-2D MHPs

Multiple phases associated with the quasi-2D MHP start to be crystallized from the precursor solution in a reservoir. The synthesized microcrystals subsequently undergo dynamic evolutions over time with a slow rate in the presence of solvent in a reservoir, without leaving kinetically-grown intermediates by solvent evaporation. This allows to *comprehensively elucidate the early-stage phase growth kinetics of the quasi-2D MHP system via simple photoluminescence (PL) characterization in the large compositional space, which cannot be deeply observed in thin-film fabrication process with advanced in-situ characterization techniques*.[17] We investigate the phase formation kinetics and evolution of 95 different quasi-2D MHP configurations by varying the 2D:3D precursor ratios in each precursor solution. Herein, we employ a modified high-throughput automated experimental workflow specifically designed to explore the compositional space of quasi-2D MHP. This workflow is developed from our well-established 3D MHP exploration workflows.[22, 23] This includes a robot-based synthesis platform, rapid PL characterization, and automated data analysis. The overall methodology is depicted in **Figure 1**, accelerating materials exploration process.

We designed a binary quasi-2D MHP system composed of 2D PEA_2PbI_4 and 3D $FAPbI_3$ end-members. Precursor solutions were prepared in a wellplate and crystallized by injecting chloroform as an antisolvent (**Figure 1a**).[12] Additionally, the dispensing rate of antisolvent into the precursor reservoir was controlled during synthesis, allowing us to investigate the effect of antisolvent injection rate which directly correlates with thin-film fabrication process via spin-

coating. The resulting wellplate, containing multiple phases of quasi-2D MHPs, was then characterized using a high-throughput fast optical reader, enabling monitoring the temporal changes in PL and phase evolutions in the quasi-2D system as a function of reaction time and 2D:3D composition ratios (**Figure 1b**). During optical characterizations, temperature of the wellplate can be precisely controlled within the range of 25-65 ^{o}C. This temperature control enables us to explore the impact of temperature in the early-stage crystallization process which can be similarly governed in thin-film annealing process, providing valuable thermodynamic insights into crystallization of quasi-2D MHPs. As an example, **Figure S1** shows PL spectra of 95 quasi-2D MHP microcrystal systems collected over 17.5 hours with a 15 min interval, consisting of 6650 individual spectra in total (95 wells in a plate × 70 measurement cycles). To analyze the large PL dataset, an automated peak fitting and tracking function was implemented (**Figure 1c)**. We then utilize a preset of rough PL characteristics for each quasi-2D phase from known physics. this facilitates efficient analysis of the PL dataset (6650 spectra in total), which automatically quantifies the intensity of each peak component associated with the corresponding 2D or 3D MHP phases. Subsequently, this allows for rendering the growth kinetics of each phase in the compositional space of the quasi-2D system. The analysis of this big data took only 5 hours in total, which is far beyond human effort alone. As a result, the proposed high-throughput experimental workflow based on the automated PL characterization is the most efficient method for comprehensive exploration in phase growth behaviors of the complex quasi-2D MHP systems.

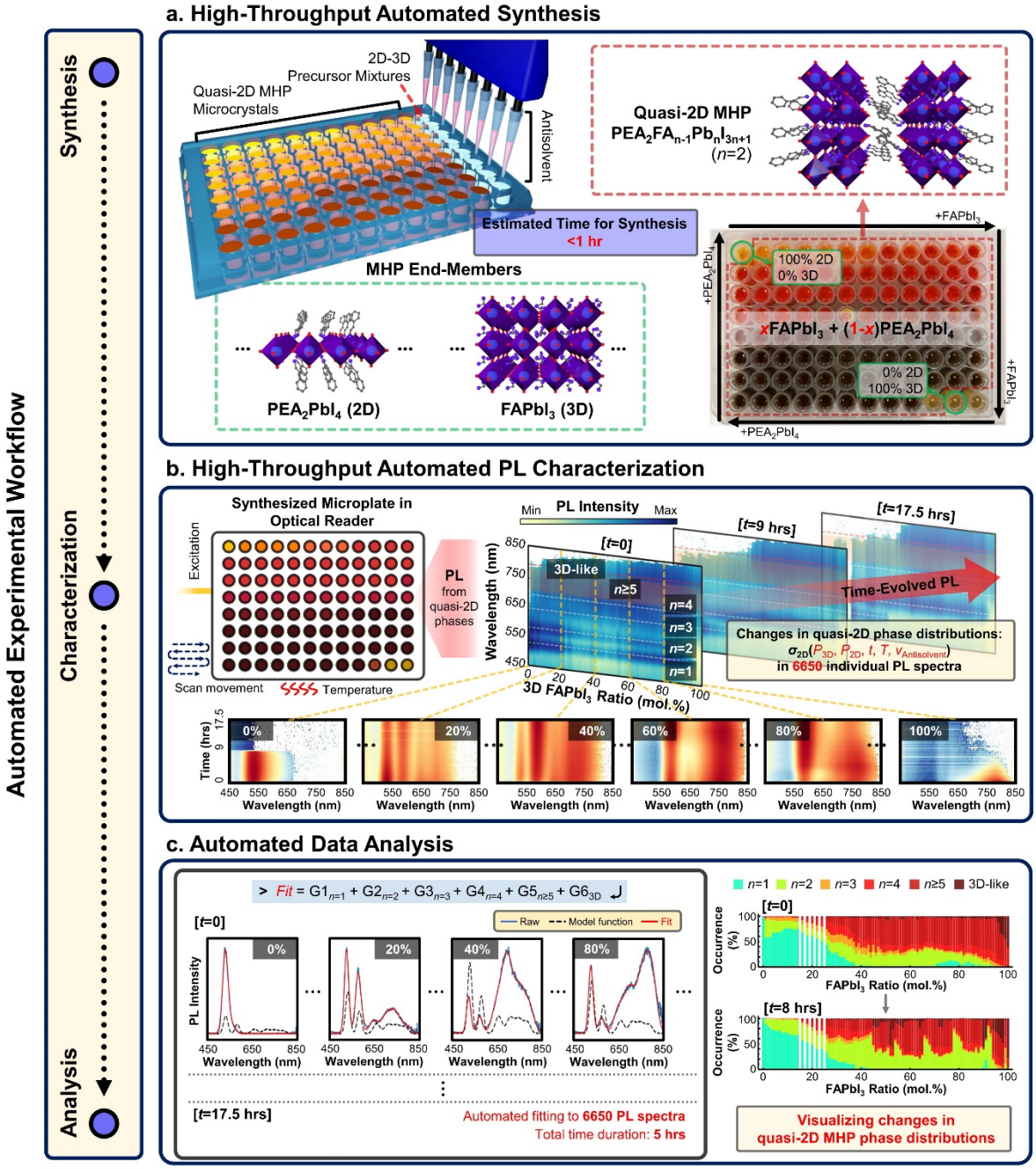

Figure 1. An automated synthesis-characterization-analysis workflow for explorations of quasi-2D MHP phase growths. (a) An illustration describing high-throughput automated synthesis of quasi-2D MHPs, with 95 different binary mixtures of 2D PEA_2PbI_4 and 3D $FAPbI_3$ end-members. The overall synthesis process can be completed within an hour. (b) High-throughput automated PL characterizations of the synthesized quasi-2D microcrystals for 20 hrs. After characterizations, a massive dataset containing 6,650 individual PL spectra (95

compositions × 70 measurement cycles; per every 15 mins for 17.5 hrs) is collected. (c) Automated data analysis of the PL dataset to distinguish and estimate the emergence of each quasi-2D phase by using a designed peak fitting function operated in Python interface. Complete assessment of the entire PL dataset takes ~5 hours, which allows us to visualize the temporal changes of the quasi-2D phases and their distributions in the system.

Figure 2a shows the PL spectral maps of the FA-based quasi-2D MHPs as a function of 3D $FAPbI_3$ composition ratios (95 in total) at three different timepoints. Regardless of the sliced timepoint, 6 distinctive PL features can be identified, each of which corresponds with one (or several) phases emerging in the quasi-2D system: 2D MHPs with inorganic layer thicknesses of n=1-4 4 (peak centered at 532, 583, 645 and 700 nm, respectively), a broadband of $n \geq 5$ quasi-2D MHPs centered at ~730-770 nm, and 3D-like MHP peak centered >780 nm, respectively. Here, the 3D-like phases indicate the 3D α-$FAPbI_3$ phase where the PEA cations are passivating the surface, which therefore exhibits negligible PL blueshift from that of pure 3D α-$FAPbI_3$. Such lattice structure is known to enhance the lattice stability, as the PEA cation can protect the MHP lattice from external stimuli.[13] The intensities of each component – with assumption that the PL intensity is proportional to the quantity of the corresponding 2D MHP phases in an ensemble – change over time (upto 17.5 hrs), suggesting a dynamic phase growth behaviors in this system.

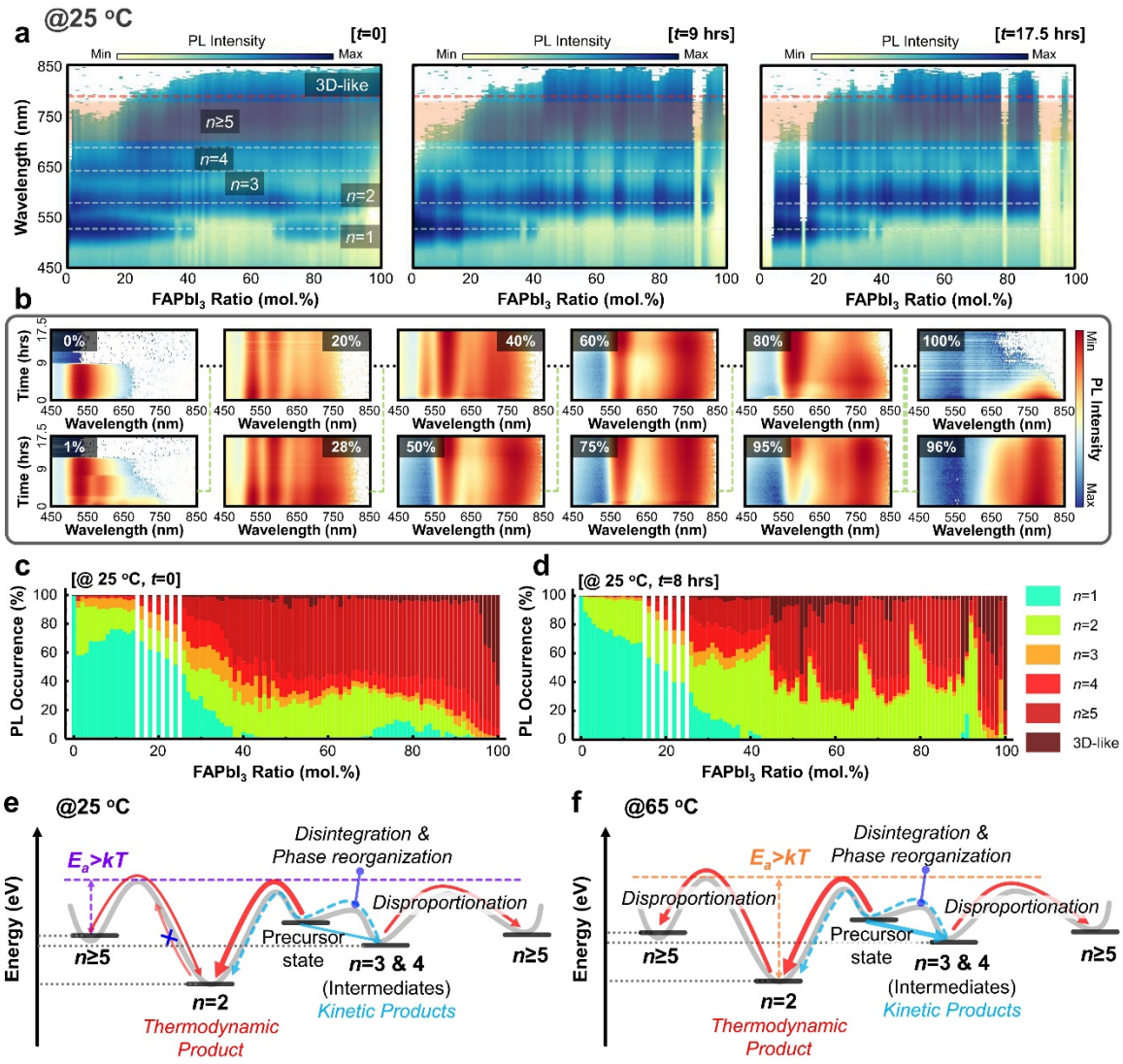

Figure 2. Phase growth behaviors of quasi-2D MHPs. (a) Snapshots of PL spectra as a function of quasi-2D MHP compositional space collected at different timepoints. (b) Time-evolved PL spectra of PEA-FA quasi-2D MHPs with selected 3D ($FAPbI_3$) compositional ratios. (c,d) quasi-2D MHP phase distributions estimated from automated peak fitting functions: (c) initial and (d) after 8 hrs from the synthesis. (e,f) Thermodynamic models describing the emergence and evolution of the FA-based quasi-2D MHP phases at (e) room temperature and (f) 65 °C, respectively.

Figure 2b shows the spectro-temporal PL maps (collected for 17.5 hrs) of the quasi-2D MHP

microcrystal ensembles with selected 3D composition ratios (corresponding time-evolved PL decay features are shown in **Figure S2**). While the single PL peak is observed over time for the MHP microcrystals with an exact *n*=1 phase stoichiometry (i.e., 0% 3D ratio; PEA_2PbI_4), multiple PL peaks emerge from the quasi-2D MHP microcrystals with 3D ratios over 1%. At 1% 3D ratio, in addition to *n*=1 2D phase, a distinctive *n*=2, as well as weak PL traces of *n*=3 and 4 2D phases emerge initially. Those PL disappear over the course of the time series, particularly the *n*=3 and 4 2D phases disappear within 3 hrs. These observations suggest that the introduction of a small amount of 3D component results in the formation of multiple 2D phases as kinetic products, but only the *n*=1 phase remains for a longer time.

Around ~20% 3D ratio, the intensity of *n*=1 PL starts to reduce over time, while the intensity of *n*=2 PL still grows over time. Meanwhile, the changes of intermediate *n*=3 and 4 PL are insignificant at 20%. Above 28% 3D ratio, it is observed that *n*=2 phase dominate over the PL spectra. At 50% 3D ratio (corresponding with *n*=2 stoichiometric condition), the *n*=2 PL dominates whereas the *n*=1 PL disappear. Even at a 95% 3D MHP ratio, the *n*=2 PL emission is still present. These results suggest a transition process from the *n*=1 to *n*=2 2D phase driven by the decomposition of the unstable *n*=1 phase, which is *irrespective to the notable disproportionation of n=3 and 4 phases in FA-based quasi-2D MHP system*.[17]

At 50% 3D ratio, it is observed that the growths of intermediate phases (i.e., *n*=3 and 4 2D MHPs) are largely suppressed and also quickly disappeared. From 96% 3D ratio, it is difficult to identify the intermediate phases. This aligns with the previous observation in FA-based quasi-2D MHP system that the intermediate phases subsequently undergo disproportionation and therefore maintaining the intermediate phases difficult unless engineering spacer cations.[17]

In addition, from 20% 3D ratio, the PL band associated with $n \geq 5$ start to emerge, which becomes dominant at 50% – compatible with that of *n*=2 phase. As the 3D ratio increases to

96%, the emission sharpens and redshifts while the *n*=2 PL disappears (**Figure S3**). This suggests that the (relatively) phase-pure 3D-like MHP can only be obtained once the *n*=2 phase is depleted, which can only be observed at high 3D composition ratios (i.e., over 96%). *The growth kinetics of the n=2 phase could obstruct the growth of the 3D-like MHP phase*.

Each peak intensity identified from the automated PL peak fitting function allows us to render an overall distribution of quasi-2D MHP phases, as shown in **Figure 2c and d** at initial timepoint and after 8 hrs. Evidently, the *n*=2 phase dominates across the quasi-2D MHP composition ratios over time. Also, the small portions of the intermediate phases are observed, which are further reduced as a result of phase disproportionation.

It is worth noting that different phase emergence behaviors are observed from MA-based quasi-2D MHP system. By using the experimental workflow onto the selected 3D ratios, we explored MA-based quasi-2D MHP system at room temperature (**Figure S4 and S5**). An evenly-distributed phase emergences are observed at both initial timepoint and after 8 hrs, showing considerable amounts of the intermediate phases. These observations implies that the dominance of *n*=2 phase and suppression of intermediate phases are exclusive features of FA-based quasi-2D MHPs. Given that the majority of the high-performance optoelectronics are based on FA-based MHPs,[17, 28, 29] understanding such non-universal features observed in this materials system is crucially important.

The A-cation site in the quasi-2D MHP lattice can be occupied by either FA or PEA. The rapid crystallization caused by antisolvent injection leads to the formation of multiple phases in the quasi-2D microcrystal system. Density-functional theory (DFT) calculations have proposed that the formation energy of quasi-2D phases increases (i.e., formation becomes difficult) with increasing *n*, with *n*=1 being the easiest phase to form.[30, 31] This is supported by the initial strong *n*=1 PL emission. The absorption spectra of solvated forms of PbI_2 in the precursor

solution (in γ-butyrolactone; GBL) are consistent for all PEA:FA ratios (**Figure S6**),[32-34] suggesting that the MHP formation reaction is independent of the precursor ratio, at least for GBL-based solution system. Over time, dynamic transformations of these quasi-2D phases result in a reorganization mainly into the *n*=2 phase. This suggests that the phase stability favors *n=2 as the most stable and preferred phase in the mixed ensemble system*.

Experimentally, we also observed that the quasi-2D MHP with 98% 3D exhibit a longer lifetime over 12 hours compared to that of pure 3D $FAPbI_3$ disappearing within 6 hours (**Figure S7**). This indicates that small incorporation of PEA spacer cation is beneficial to enhance the stability of α-$FAPbI_3$ phase,[13] which is not thermodynamically stable at room temperature.[25] These observations are consistent with previous reports in the thin film system, where the PEA spacer passivates the 3D MHP surface and protects the lattice against external stresses.[4, 13]

To further explore the thermodynamic insights into the quasi-2D phase growth behaviors, we studied the evolution of phase growth at an elevated temperature of 65 °C during PL characterizations for 4 hrs (**Figure S8 and S9**) by using a temperature control function equipped in the optical reader. The higher temperature results in the increase of kinetic energy in the overall system, which accelerates the reaction kinetics. Initially, we observed the larger portions of the intermediate phases, particularly *n*=4 MHP, which becomes larger over time. This can be explained by a facilitated growth of the kinetic products as a result of the increased kinetic energy at an elevated temperature. Additionally, *n*=4 and *n*≥5 phases become dominant at the expense of the emergence of the *n*=2 phase. **Figure S10a** exhibit histograms of the wavelength at the strongest PL peak in each spectrum of the datasets collected at 25 °C and 65 °C. Clearly, suppression on *n*=2 phases and increases of *n*=4 and *n*≥5 phases are observed at a higher temperature (**Figure S10b**). This implies that, rather than intermediate phases, *n*=2 phase – stable at room temperature – starts to disproportionate and transform to high-*n* phases.

Combining these observations with the formation energy proposed by previous DFT calculations,[30] we establish a plausible thermodynamic model describing the observed phase growth behaviors of the FA-based quasi 2D MHP system (**Figure 2e and 2f**). From the precursor state, all 2D phases can be formed initially, as the kinetic energy at room temperature is enough to overcome the activation barriers required for each phase. Due to the low activation barrier, the intermediate phases can be kinetically formed, however these phases subsequently undergo disproportionation to be merged to $n \geq 5$ phase or directed to $n=2$ phase. However, it is difficult for the thermodynamically most stable $n=2$ phase to undergo disproportination, given the large activation barrier towards the formation of $n \geq 5$ (**Figure 2e**). This rationalize why the $n=2$ phase dominates the overall quasi-2D MHP system. At higher temperature, however, the kinetic energy becomes sufficient to overcome the activation barrier for the disproportionation of $n=2$ phase and subsequent formation of $n \geq 5$ phase (**Figure 2f**). This can allow evolution of $n=2$ phase to $n \geq 5$ MHPs, justifying our observations.

In addition, we explored the effect of antisolvent injection rate – a crucial factor determining the quality of MHPs[35] – by controlling the dispensing rate of antisolvent injection for high-throughput quasi-2D MHP synthesis in robotic platform operated under Python interface. This allows us to gain practical insights into the processing-property relationship for obtaining high quality quasi-2D MHPs. We employed a slow antisolvent dispensing rate (40 μL/sec) during high-throughput automated synthesis (**Figure S11 and S12**). Notably, the larger portions of intermediate phases were initially observed at the expense of the emergence of $n=2$ phase. The slow antisolvent injection manifests the nucleation takes place for a longer time, thereby increasing the number of kinetic products. After 8 hours, those intermediate phases almost disappeared and $n=2$ phase dominates over the quasi-2D MHP compositional space, even with a larger portion compared to that obtained from the fast antisolvent injection. These results also corroborates our hypothesis of thermodynamic model, thus suggesting that slow antisolvent

injection is inferior to manifest 3D-like phase. Nevertheless, we note there are special demands on the realization of the intermediate phases for red light-emitting diode applications. Given that the large spacer cation can effectively suppress the disproportionation and thereby maintain the intermediate phases,[17] the slow antisolvent injection can lead to a synergistic effect in this regard.

Overall, high-throughput exploration of quasi-2D MHP compositional space uncovers the early-stage phase formation and growth kinetics in solution phase, which could not be properly observed from device-level or even in-situ film characterizations. We reveal that, among the multiple quasi-2D phases, n=2 MHP is the most stable phase and preferentially formed at the early-stage of MHP crystallization. Furthermore, the growth kinetics of n=2 phases dominates the quasi-2D MHP compositional space, leaving broad distributions of higher-n ($n\geq5$) phases and suppressing the growth of the 3D-like phase. This not only manifests the energetic disorder in the system but also restricts the growth of the functional 3D-like phases, both limiting the optoelectronic performances – particularly in PV applications.[36] The use of high temperature suppresses the n=2 phase and facilitates the growths of intermediate phases and $n\geq5$ phases, suggesting that complicated thermodynamic relationships between each 2D MHPs are entangled in this system. The control over the antisolvent dispensing rate further provides practical insights into the control of quasi-2D MHP emergences, where the slow rate is beneficial to manifest intermediate phases.

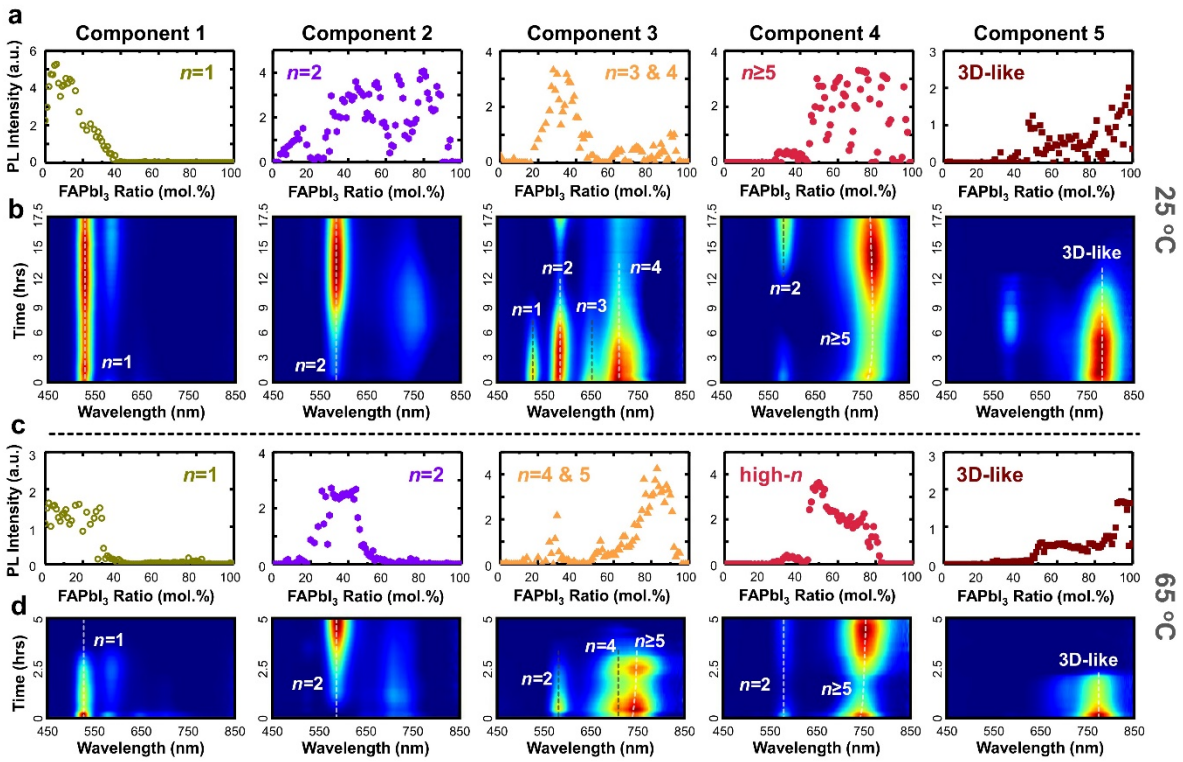

Figure 3. NMF Analysis. (a) PL loading maps and (b) the characteristic spectro-temporal PL profiles (collected at 25 °C) of each NMF component – illustrating the emergence of each phase in quasi-2D MHPs: n=1, n=2, n=3&4, high-n (n≥5) and 3D-like phase, respectively. (c) PL loading maps and (d) the characteristic spectro-temporal PL profiles (collected at 65 °C) of each NMF component – illustrating the emergence of each phase in quasi-2D MHPs: n=1, n=2, n=3&4, high-n (n≥5) and 3D-like phase, respectively.

Multivariate analysis using non-negative matrix factorization (NMF) was applied to analyze the PL datasets of the quasi-2D MHP system.[23] This method allows for the extraction of key dynamics related to phase growth kinetics and the mapping of time- and composition-dependent PL evolution in the system. Five components were optimally chosen from the analysis: n=1, n=2, intermediate n (n=3 and 4), high-n (n≥5, PL peak wavelength <~780 nm), and 3D-like (PL peak >780 nm), as shown in **Figure 3a and b**. As the 3D ratio increases, the

intensity of the *n*=1 phase decreases and eventually disappears at a 3D ratio of around 40%. In contrast, the *n*=2 phase emerges throughout all 3D compositions. The intermediate phases emerge in the 3D ratio range of 20-50%, which almost disappeared quicker than the other phases. The high-*n* (*n*≥5) phases, accompanied by the *n*=2 phase, develops from the 3D ratio of 50%. 3D-like phase also start to emerge from 40%, which rapidly increases in intensity over 90%, unveiling the optimal compositional range to get 3D-like phase rich MHP system. The PL dataset collected at 65 ^{o}C was also deconvoluted with the same way (**Figure 3c and d**). Notably, the compositional range where *n*=2 phase emerges (accompanied with a weak signal of intermediate phases) is confined within 20-50%. Meanwhile, the emergence of intermediate phases including partial *n*≥5 phases (peak center <750 nm) gradually increase from 60% 3D ratio and peaked at ~85%. Given the high-*n* phases (≥5, peak center >750 nm) emerge at a distinctive 3D compositional range from 40-80%, this could be attributed to the disproportionation of the high-*n* phases. The phase emergence of 3D-like phase exhibits similar trend with that observed at 25 ^{o}C. This unsupervised machine learning approach confirms the overall behaviors of the studied quasi-2D system with the observations made through automated peak fitting, emphasizing its usefulness in the data analysis of high-throughput experiments.

Emerging features of quasi-2D MHPs in thin films

To further explore how the initially determined quasi-2D phases at the early-stage of crystallization evolve during film fabrication process, phase evolutions of quasi-2D MHPs in thin films are investigated. Based on our high-throughput synthesis, we selected 6 ratios of 2D:3D, prepared them as thin films using the same conditions (**Figure S13a**), and similarly studied the evolution of PL behavior. The PL results show that the *n*=2 phase is present in the

films up to 50% 3D ratios while the *n*=1 is absent. Even in the film with 67% 3D ratio, the *n*=2 phase remains, which is confirmed by the corresponding XRD patterns and absorption spectrum (**Figure S14 and S15**). Note that, for this film, the *n*=2 phase cannot be seen from the PL spectra (**Figure S13e**), attributed to energy transfer to the vicinal higher-*n* phase,[3, 9-12] Meanwhile, the high-*n* (*n*≥5) phases emerge in the films with 3D ratio over 50%, where the corresponding PL band gradually broadened or redshifted over time, likely attributed to the disproportionation of *n*=3~4 phases upon film drying. Note that the overall phase constitutions are analogous to those observed in the microcrystal system, indicating the major phases in the films are primarily determined at the early-stage of phase formation. The use of molecularly tailored spacers and associated organic-inorganic interaction could control the early-stage phase growth kinetics,[17] thereby beneficial to achieve phase-pure quasi-2D system.

In contrast to the microcrystals in the solution phase, thermal annealing was found to be necessary for the formation of higher-*n* and 3D-like phases in the thin films (**Supplementary Note 1**, **Figure S13-15**). This was likely due to the formation of the δ-$FAPbI_3$ phase at room temperature,[25, 37] which impedes the formation of the 3D-like phase – a structure of α-$FAPbI_3$ MHP lattice where the spacers are coordinated to the surface. X-ray diffraction (XRD) patterns of the films show no appreciable peaks associated with the solvent-intermediate phase (**Figure S15a**),[38] ruling out the influence of the solvent on MHP crystallization. Additionally, thermal annealing induces disproportionation of intermediate phases that results in higher-*n* phases,[17] at the expense of emergence of *n*=1 (for 1% and 28% 3D ratio) or *n*=2 (for 50% and 67% 3D raio) phases.

Local phase inhomogeneities in the quasi-2D MHP films were explored using hyperspectral CL microscopy (**Supplementary Note 2, Figure S16-18**).[39] The CL maps of 2D MHPs are strongly homogeneous. However, it is observed that local PbI_2 crystallites emerge on the

surface of quasi 2D MHPs after annealing. These results indicate that thermal annealing is necessary for the formation of functional 3D-like α-$FAPbI_3$ phase, but it also results in the emergence of local PbI_2 crystallites, which may negatively impact device performance.[27, 39] Given that the pure PEA_2PbI_4 is stable up to 250 °C,[40] the incomplete evaporation of solvent in the film before annealing may support thermal disproportionation and decomposition of the lower-*n* phases. Some of the disintegrated ions may be diffused into the higher-*n* lattice, induce ripening of the 3D-like phase[41] or passivate internal defects that results in temporal PL enhancements – observed from the films with 92 and 98% 3D ratios. Meanwhile, the remainder left as PbI_2 (and/or δ-$FAPbI_3$) byproducts.

Figure 4 provides a general schematic of the fate of associated phases in the quasi-2D MHP, offering a comprehensive guide for designing the functional system. Before annealing, the phase distributions in the films are majorly defined at the early-stage of growth process, as observed in microcrystal systems. At high 3D ratios, thermodynamically stable δ-$FAPbI_3$ emerges and suppresses the growth of 3D-like phase. Thermal annealing enables them to transform to the 3D-like phase and improves crystallinity. However, it also induces lattice disproportionation, which not only results in higher-*n* phases at the expense of intermediate *n*=2-4 phases but also leaves local PbI_2 byproducts. The resulting broader phase distributions and the impurity phases can limit the optoelectronic performances.[27, 39]

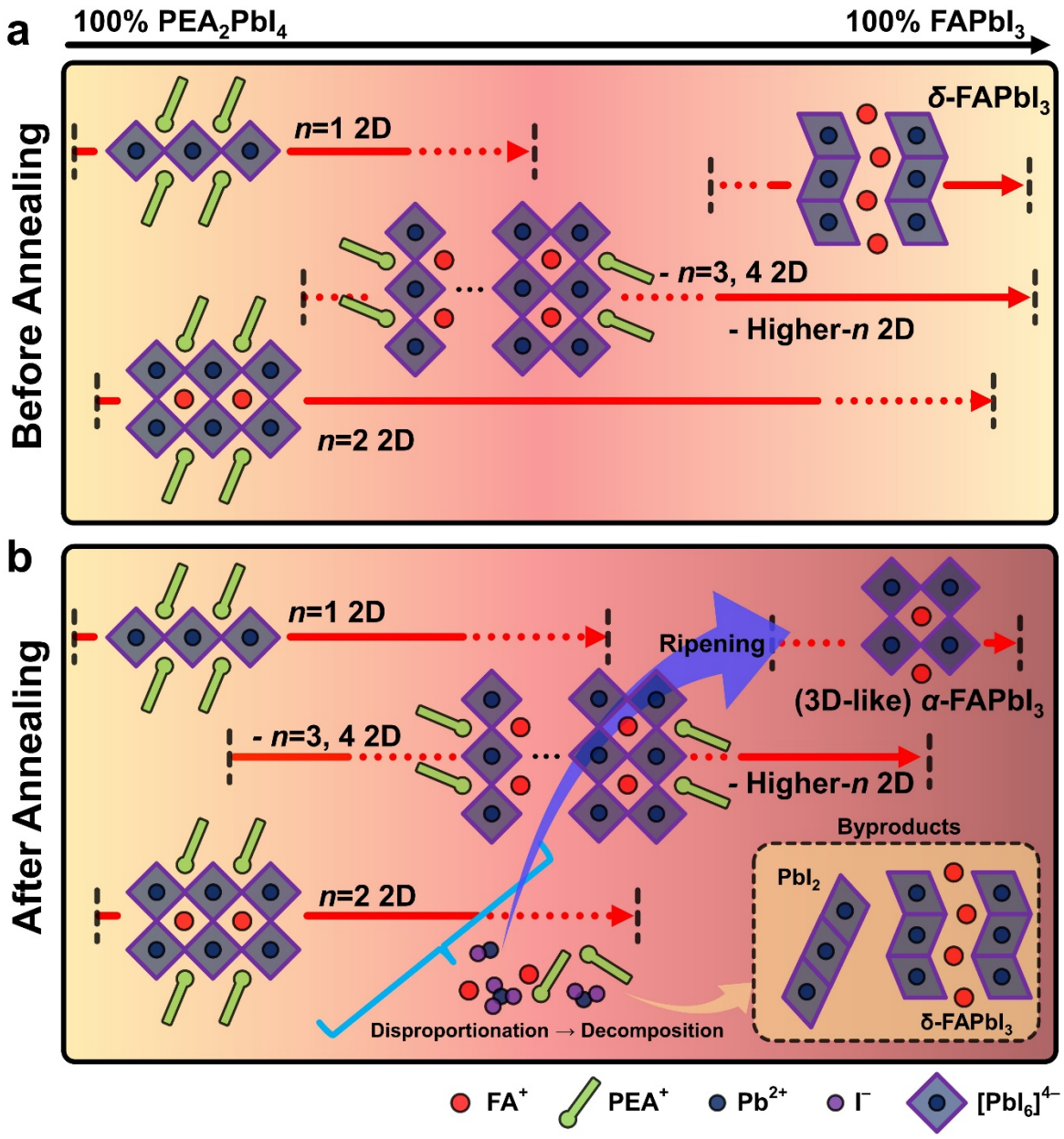

Figure 4. Overall Phase emergence landscape of PEA-FA quasi-2D MHP system. (a,b) Schematic of phase distribution and growth behaviors in PEA-FA quasi-2D MHP film system in a 2D:3D compositional space: (a) before and (b) after annealing. The initial phase distributions are defined at the early-stage phase growth process, as seen in microcrystal system. At high 3D ratios, thermodynamically stable δ-$FAPbI_3$ emerges. By annealing the films, higher-*n* and 3D-like phases are formed at the expense of intermediate *n*=2-4 2D phases via disproportionation, which also leaves the unwanted PbI_2 byproduct.

Influence of solvent on the phase distribution of quasi-2D MHP

Solvents play a crucial role in shaping the surface morphology and crystallinity of the resulting MHP films due to their interaction with the precursor solutes.[32-34, 38] Hence, we increased the concentration of MHP precursors to the nominal level for optoelectronic device fabrication and studied the impact of solvent on the phase formation in quasi-2D MHP films (**Figure S19**). For films with 28% 3D ratio, along with the growth of the *n*=1 phase, higher-*n* phases emerge by using more coordinative solvents in the order of GBL < DMF < DMSO (**Figure 5a-c and S20**). The emission from the *n*=1 phase became stronger with increasing Lewis basicity of the solvent (DMSO), in agreement with the trend of growing *n*=1 2D diffraction peak (**Figure S21**). These observations suggest that the disproportionation of the intermediate-*n* phases (particularly *n*=2 phase in this case) is promoted by the coordinative solvents. This has been explained by the increase of nucleation barrier of quasi-2D phases, collectively attributed to the formation of PbI_2-solvent adduct and strong spacer-solvent interaction.[42] The polar nature of PEA cation, with a dipole moment of ~14.0 Debye results in strong hydrogen bond with the Lewis base DMSO, inhibiting the 2D phase formation.[42, 43] In contrast, FA has a weak polarity (dipole moment of 0.25 Debye) and therefore the nucleation of 3D phase can be relatively feasible.[44] We collected absorption spectra of 2D and 3D precursor solutions to assess the iodoplumbate formation in the solution phase (**Figure S22**). Indeed, with increasing coordinative character of the solvent, notable imbalance in ionic forms between the 2D and 3D precursors is observed,[33] with the 3D precursor exhibiting more disintegrated forms than the 2D precursor. This results in the broader phase distributions with higher-*n* phases in PL spectra.

At 3D ratios up to 67%, a preferential product i.e., the *n*=2 phase, appears along with a 3D-like phase. At a 3D ratio of 98%, only the single peak of α-$FAPbI_3$ is observed in the films,

regardless of the solvent used, with superior crystallinity compared to pure 3D MHP (sharper XRD peak, **Figure S21**). Particularly, the films produced using the DMF and DMF:DMSO solvent systems show large and smooth MHP grains as seen by scanning electron microscopy (**Figure S23**), showing notable difference with those of pure 3D films. However, the overall surface morphology of the 98% MHP film produced using only DMF is poor – presumably due to fast vaporization of the solvent,[45] suggesting that DMF is not compatible for making films with high 3D compositional ratios. The addition of DMSO improves the morphology. We hypothesize that the difference in solute-solvent interaction between 2D and 3D solutions is associated with these results (**Figure S22**). The heterogeneous solvation of precursor ions in different solvents would cause different nucleation kinetics in 2D and 3D phases,[42] where the larger difference (in this case, DMF) could infer the kinetic imbalance and subsequently result in the irregular morphology. For DMF:DMSO mixed solvent system, although there is still an imbalance of precursor solvation, the strong hydrogen bonding between the spacer and DMSO can inhibit the 2D phase growth and promote the selective crystallization and coarsening of 3D phases.[42] As a result, this can renders larger 3D MHP grains,[46] whereas the residual 2D precursors smoothen and passivate the 3D grain surfaces – analogous to the observations in 3D MHPs incorporating alkylammonium salts.[28, 46]

Indeed, Fourier-transform infrared (FTIR) spectroscopy analysis reveals that solvent dominantly interacts with organic cations – stronger for 2D spacer cation compared to 3D counterpart – than PbI_2 (**Figure 5g, 5h, and S24**). Particularly, there are hydrogen bonding interactions between DMSO and organic cations (reflected as peak broadening),[47, 48] which likely cause imbalanced solvation of the precursors as seen in **Figure S22**.

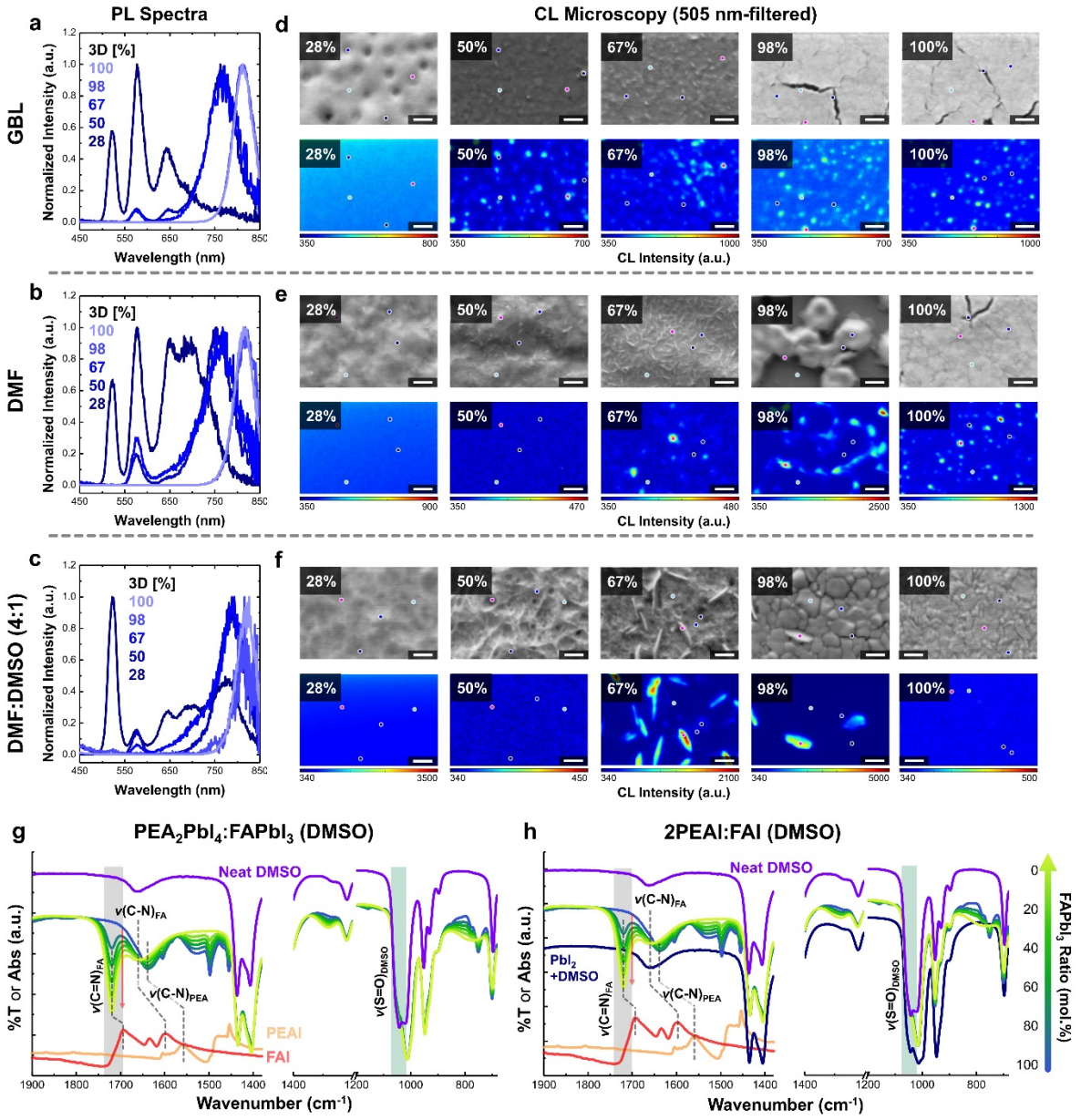

Figure 5. Local phase inhomogeneities of quasi-2D MHPs associated with chemical interactions in precursor solution. (a-c) PL spectra, (d-f) SEM and 505 nm-filtered CL maps (assigned to PbI_2) for the quasi-2D MHPs films with different solvent systems. All films were prepared by annealing the spin-casted substrates at 150 °C for 20 min (Scale bar: 1 μm). Four local spots are chosen and color-marked in the map, where the corresponding CL spectra are shown in **Figure S25**. (g,h) FTIR spectra of (g) quasi-2D MHP precursor and (h) organic cation solutions with different 2D:3D ratios in DMSO. For convenience, FTIR spectra of neat solvents,

as well as PEAI and FAI powders are also included.

From the CL analysis, the presence of local PbI_2 crystallites (505 nm CL) in the films is again observed (**Figure 5d-f** and **S25**), with larger sizes seen when DMSO is added in the solvent mixture. While DMSO can make PbI_2-DMSO adducts, it can strongly coordinate with PEA cation via hydrogen bonding inhibiting the 2D phase growth.[42] Experimentally, we observed that the interaction between the PEA cation and solvent – particularly in DMSO – is substantial, overwhelming that of PbI_2 (**Figure 5g, 5h, and S24**). After annealing, the residual adducts, after consuming all FA cations to form $FAPbI_3$ first, could be left. While some of the PEA spacers are used to render smooth 3D MHP grains upon crystallization from the solvated ion precursors,[28] considerable amount of the spacer can be stripped out with the solvent during spin coating process. the remaining (PbI_2-rich) 2D precursor adducts are subsequently transform into large PbI_2 aggregates or PEA-poor, defective 2D phases that readily undergo lattice disproportionation (**Figure S26**). Relatively weaker coordination of DMF could be responsible for the smaller size of PbI_2 crystallites. Meanwhile, the poor surface morphology particularly at 98% 3D ratio could also lead to extrusion of PbI_2 alongside the grain exteriors.

A strong 745 nm CL band, which is not detected in photoluminescence analysis, is also observed in films with high 3D ratios (98% and 100%), particularly at grain boundaries or wrinkled surface structures (**Figure S27**). This is attributed to the CL emission from the photoinactive δ-$FAPbI_3$, rather than other low-dimensional $FAPbI_3$ polymorphs,[49, 50] as no significant XRD peaks of the latter are observed. We note that this CL band becomes stronger with increasing the coordinative character of the solvent, which also involves rougher surface morphology with more amounts of wrinkled structures. We hypothesize that the coarse surface edges at the grain boundary and the microstructures – possibly with larger amounts of surface defects[51] – could readily be transformed to the δ-$FAPbI_3$ phase.

Summarizing, the strong chemical interaction between the solvent and precursors leads to significant changes in surface morphology, microstructures, phase distributions and emergence of secondary phases in the quasi-2D MHP films. The spacer cation, due to its high polarity, strongly interact with solvent, where the chemical interaction is proportional to the coordinative strength of the solvent. The increase of solvent-spacer interaction strength can induce an imbalanced solvation of 2D and 3D components in precursor solutions. Subsequently, this lacks the amounts of 'activated' 2D spacer cations and largely complicates the MHP crystallization behaviors associated with the surface morphologies, phase inhomogeneities, local microstructures in the films. Solving such complexities requires multimodal approaches including molecular tailoring of the spacers and solvent engineering. High-throughput exploration of the early-stage phase growth kinetics of quasi-2D MHPs and hyperspectral CL microscopy reveal indispensable features and principles associated with the system, which could not be conventionally observed. In turns, these findings provide crucial insights for optimization and development of the functional quasi-2D MHP system.

Conclusion

In summary, the phase growth kinetics of PEA-FA quasi-2D MHPs are systematically explored using an automated experimental workflow based on high-throughput automated synthesis, optical characterization and spectral analysis. Without relying on manual intervention, this allows for efficiently monitoring the early-stage phase growth kinetics of 95 different microcrystal ensembles in a quasi-2D MHP compositional space, which could not be properly observed from the conventional film fabrication protocols.

Experimentally, the most preferentially formed and stable phase is found to be the n=2 2D phase, which is irrespective to the disproportionation of kinetically-grown products and

prominent in the overall compositional space. Furthermore, the $n \geq 5$ phases emerge with increasing 3D ratio up to 95%, as a result of the restricted growth of 3D-like phase by $n=2$ phase; the stable 3D-like phase can be observed after the $n=2$ phase is depleted (from 96%).[13]

Characterizations of the quasi-2D MHP films reveal that the presence of thermodynamically stable δ-$FAPbI_3$ also hinders the formation of the 3D-like phase. Thermal annealing transforms the non-perovskite phase to photoactive α-$FAPbI_3$, thereby allowing the emergence of the 3D-like phase. However, hyperspectral analysis also revealed the emergence of locally formed PbI_2 crystallites, presumably due to thermal-assisted disproportionation; this impurity phase is known to negatively impact MHP functionality[27] but difficult to be identified via conventional analysis such as PL and XRD.[39] Furthermore, it is revealed that the choice of spacer cations and solvent system – due to the strong chemical interaction with each other – crucially impacts the phase distributions, surface morphologies and local phase inhomogeneities, necessitating judicious considerations of molecular and solvent engineering. These new findings provide crucial insights into the phase distributions and growth kinetics in quasi-2D MHP systems, important for optimizing MHP functionality. Furthermore, the powerfulness of the integrated workflow utilized in this work enables us to accelerate of materials discovery, processing optimization, and comprehensive mechanistic study in other functional systems in future.

Acknowledgements

J.Y. and M.A acknowledge support from National Science Foundation (NSF), Award Number No. 2043205 and Alfred P. Sloan Foundation, award No. FG-2022-18275. The CL microscopy was supported by the Center for Nanophase Materials Sciences (CNMS) user facility, project CNMS2022-A-01171, which is a US Department of Energy, Office of Science User Facility at Oak Ridge National Laboratory.

Data availability

The PL dataset of high-throughput synthesized microcrystals is available in the provided code. The other datasets including absorption spectra, XRD patterns, and hyperspectral CL microscopy can be found in Figshare (https://doi.org/10.6084/m9.figshare.22350910.v1).

Code availability

The Python codes used for the high-throughput PL dataset are available in google Colab: https://drive.google.com/file/d/1uVp0G2-m6HWFQPFFRa1-V1bmQqhef3wu/view?usp=sharing

References

1. Min, H.; Lee, D. Y.; Kim, J.; Kim, G.; Lee, K. S.; Kim, J.; Paik, M. J.; Kim, Y. K.; Kim, K. S.; Kim, M. G.; Shin, T. J.; Il Seok, S., Perovskite solar cells with atomically coherent interlayers on SnO2 electrodes. *Nature* **2021,** *598* (7881), 444-450.
2. Hassan, Y.; Park, J. H.; Crawford, M. L.; Sadhanala, A.; Lee, J.; Sadighian, J. C.; Mosconi, E.; Shivanna, R.; Radicchi, E.; Jeong, M.; Yang, C.; Choi, H.; Park, S. H.; Song, M. H.; De Angelis, F.; Wong, C. Y.; Friend, R. H.; Lee, B. R.; Snaith, H. J., Ligand-engineered bandgap stability in mixed-halide perovskite LEDs. *Nature* **2021,** *591* (7848), 72-77.
3. Ma, D.; Lin, K.; Dong, Y.; Choubisa, H.; Proppe, A. H.; Wu, D.; Wang, Y. K.; Chen, B.; Li, P.; Fan, J. Z.; Yuan, F.; Johnston, A.; Liu, Y.; Kang, Y.; Lu, Z. H.; Wei, Z.; Sargent, E. H., Distribution control enables efficient reduced-dimensional perovskite LEDs. *Nature* **2021,** *599* (7886), 594-598.
4. Boyd, C. C.; Cheacharoen, R.; Leijtens, T.; McGehee, M. D., Understanding Degradation Mechanisms and Improving Stability of Perovskite Photovoltaics. *Chem Rev* **2019,** *119* (5), 3418-3451.

5. Jeong, J.; Kim, M.; Seo, J.; Lu, H.; Ahlawat, P.; Mishra, A.; Yang, Y.; Hope, M. A.; Eickemeyer, F. T.; Kim, M.; Yoon, Y. J.; Choi, I. W.; Darwich, B. P.; Choi, S. J.; Jo, Y.; Lee, J. H.; Walker, B.; Zakeeruddin, S. M.; Emsley, L.; Rothlisberger, U.; Hagfeldt, A.; Kim, D. S.; Gratzel, M.; Kim, J. Y., Pseudo-halide anion engineering for α-$FAPbI_3$ perovskite solar cells. *Nature* **2021,** *592* (7854), 381-385.
6. Blancon, J. C.; Even, J.; Stoumpos, C. C.; Kanatzidis, M. G.; Mohite, A. D., Semiconductor physics of organic-inorganic 2D halide perovskites. *Nature Nanotechnology* **2020,** *15* (12), 969-985.
7. Soe, C. M. M.; Nagabhushana, G. P.; Shivaramaiah, R.; Tsai, H. H.; Nie, W. Y.; Blancon, J. C.; Melkonyan, F.; Cao, D. H.; Traore, B.; Pedesseau, L.; Kepenekian, M.; Katan, C.; Even, J.; Marks, T. J.; Navrotsky, A.; Mohite, A. D.; Stoumpos, C. C.; Kanatzidis, M. G., Structural and thermodynamic limits of layer thickness in 2D halide perovskites. *P Natl Acad Sci USA* **2019,** *116* (1), 58-66.
8. Li, X. T.; Hoffman, J. M.; Kanatzidis, M. G., The 2D Halide Perovskite Rulebook: How the Spacer Influences Everything from the Structure to Optoelectronic Device Efficiency. *Chemical Reviews* **2021,** *121* (4), 2230-2291.
9. Gan, X.; Chen, W.; Liu, C.; Zhang, J.; Di, Y.; Yu, L.; Dong, L.; Jia, B.; Wen, X., Energy Funneling in Quasi-2D Ruddlesden–Popper Perovskites: Charge Transfer versus Resonant Energy Transfer. *Adv Photonics Res* **2022,** *3*, 2100283.
10. Yuan, M.; Quan, L. N.; Comin, R.; Walters, G.; Sabatini, R.; Voznyy, O.; Hoogland, S.; Zhao, Y.; Beauregard, E. M.; Kanjanaboos, P.; Lu, Z.; Kim, D. H.; Sargent, E. H., Perovskite energy funnels for efficient light-emitting diodes. *Nat Nanotechnol* **2016,** *11* (10), 872-877.
11. Quan, L. N.; Zhao, Y.; Garcia de Arquer, F. P.; Sabatini, R.; Walters, G.; Voznyy, O.; Comin, R.; Li, Y.; Fan, J. Z.; Tan, H.; Pan, J.; Yuan, M.; Bakr, O. M.; Lu, Z.; Kim, D. H.; Sargent, E. H., Tailoring the Energy Landscape in Quasi-2D Halide Perovskites Enables Efficient Green-Light Emission. *Nano Lett* **2017,** *17* (6), 3701-3709.
12. Quan, L.; Ma, D. X.; Zhao, Y. B.; Voznyy, O.; Yuan, H. F.; Bladt, E.; Pan, J.; de Arquer, F. P. G.; Sabatini, R.; Piontkowski, Z.; Emwas, A. H.; Todorovic, P.; Quintero-Bermudez, R.; Walters, G.; Fan, J. Z.; Liu, M. X.; Tan, H. R.; Saidaminov, M. I.; Gao, L.; Li, Y. Y.; Anjum, D. H.; Wei, N. N.; Tang, J.; McCamant, D. W.; Roeffaers, M. B. J.; Bals, S.; Hofkens, J.; Bakr, O. M.; Lu, Z. H.; Sargent, E. H., Edge stabilization in reduced-dimensional perovskites. *Nature Communications* **2020,** *11* (1).
13. Lee, J. W.; Dai, Z.; Han, T. H.; Choi, C.; Chang, S. Y.; Lee, S. J.; De Marco, N.; Zhao, H.; Sun, P.; Huang, Y.; Yang, Y., 2D perovskite stabilized phase-pure formamidinium perovskite solar cells. *Nat Commun* **2018,** *9* (1), 3021.

14. Sidhik, S.; Wang, Y.; De Siena, M.; Asadpour, R.; Torma, A. J.; Terlier, T.; Ho, K.; Li, W.; Puthirath, A. B.; Shuai, X.; Agrawal, A.; Traore, B.; Jones, M.; Giridharagopal, R.; Ajayan, P. M.; Strzalka, J.; Ginger, D. S.; Katan, C.; Alam, M. A.; Even, J.; Kanatzidis, M. G.; Mohite, A. D., Deterministic fabrication of 3D/2D perovskite bilayer stacks for durable and efficient solar cells. *Science* **2022,** *377* (6613), 1425-1430.
15. Zhang, F.; Park, S. Y.; Yao, C.; Lu, H.; Dunfield, S. P.; Xiao, C.; Ulicna, S.; Zhao, X.; Du Hill, L.; Chen, X.; Wang, X.; Mundt, L. E.; Stone, K. H.; Schelhas, L. T.; Teeter, G.; Parkin, S.; Ratcliff, E. L.; Loo, Y. L.; Berry, J. J.; Beard, M. C.; Yan, Y.; Larson, B. W.; Zhu, K., Metastable Dion-Jacobson 2D structure enables efficient and stable perovskite solar cells. *Science* **2022,** *375* (6576), 71-76.
16. Sun, C.; Jiang, Y.; Cui, M.; Qiao, L.; Wei, J.; Huang, Y.; Zhang, L.; He, T.; Li, S.; Hsu, H. Y.; Qin, C.; Long, R.; Yuan, M., High-performance large-area quasi-2D perovskite light-emitting diodes. *Nat Commun* **2021,** *12* (1), 2207.
17. Wang, K.; Lin, Z. Y.; Zhang, Z.; Jin, L.; Ma, K.; Coffey, A. H.; Atapattu, H. R.; Gao, Y.; Park, J. Y.; Wei, Z.; Finkenauer, B. P.; Zhu, C.; Meng, X.; Chowdhury, S. N.; Chen, Z.; Terlier, T.; Do, T. H.; Yao, Y.; Graham, K. R.; Boltasseva, A.; Guo, T. F.; Huang, L.; Gao, H.; Savoie, B. M.; Dou, L., Suppressing phase disproportionation in quasi-2D perovskite light-emitting diodes. *Nat Commun* **2023,** *14* (1), 397.
18. Sanchez, S. L.; Tang, Y.; Hu, B.; Yang, J.; Ahmadi, M., Understanding the ligand-assisted reprecipitation of CsPbBr3 nanocrystals via high-throughput robotic synthesis approach. *Matter* **2023**.
19. Yang, J.; Kalinin, S. V.; Cubuk, E. D.; Ziatdinov, M.; Ahmadi, M., Toward self-organizing low-dimensional organic-inorganic hybrid perovskites_Machine learning-driven co-navigation of chemical and compositional spaces. *MRS Bull* **2023,** *48*.
20. Zhang, J.; Langner, S.; Wu, J.; Kupfer, C.; Luer, L.; Meng, W.; Zhao, B.; Liu, C.; Daum, M.; Osvet, A.; Li, N.; Halik, M.; Stubhan, T.; Zhao, Y.; Hauch, J.; Brabec, C. J., Intercalating-Organic-Cation-Induced Stability Bowing in Quasi-2D Metal-Halide Perovskites. *ACS Energy Letters* **2022,** *7*, 70-77.
21. Zhao, Y.; Hueumaueller, T.; Zhang, J.; Luo, J.; Kasian, O.; Langner, S.; Kupfer, C.; Liu, B.; Zhong, Y.; Elia, J.; Osvet, A.; Wu, J.; Liu, C.; Wan, Z.; Jia, C.; Li, N.; Hauch, J.; Brabec, C. J., A bilayer conducting polymer structure for planar perovskite solar cells with over 1400 hours operational stability at elevated temperatures. *Nat Energy* **2022,** *7*, 144-152.
22. Higgins, K.; Valleti, S. M.; Ziatdinov, M.; Kalinin, S. V.; Ahmadi, M., Chemical Robotics Enabled Exploration of Stability in Multicomponent Lead Halide Perovskites via Machine Learning. *Acs Energy Letters* **2020,** *5* (11), 3426-3436.

23. Higgins, K.; Ziatdinov, M.; Kalinin, S. V.; Ahmadi, M., High-Throughput Study of Antisolvents on the Stability of Multicomponent Metal Halide Perovskites through Robotics-Based Synthesis and Machine Learning Approaches. *J Am Chem Soc* **2021,** *143* (47), 19945-19955.
24. Long, H.; Peng, X.; Lu, J.; Lin, K.; Xie, L.; Zhang, B.; Ying, L.; Wei, Z., Exciton–phonon interaction in quasi-two dimensional layered (PEA)2(CsPbBr3)n−1PbBr4 perovskite. *Nanoscale* **2019,** *11*, 21867-21871.
25. Pool, V. L.; Dou, B.; Van Campen, D. G.; Klein-Stockert, T. R.; Barnes, F. S.; Shaheen, S. E.; Ahmad, M. I.; van Hest, M. F.; Toney, M. F., Thermal engineering of FAPbI3 perovskite material via radiative thermal annealing and in situ XRD. *Nat Commun* **2017,** *8*, 14075.
26. Milic, J. V.; Zakeeruddin, S. M.; Gratzel, M., Layered Hybrid Formamidinium Lead Iodide Perovskites: Challenges and Opportunities. *Acc Chem Res* **2021,** *54* (12), 2729-2740.
27. Macpherson, S.; Doherty, T. A. S.; Winchester, A. J.; Kosar, S.; Johnstone, D. N.; Chiang, Y. H.; Galkowski, K.; Anaya, M.; Frohna, K.; Iqbal, A. N.; Nagane, S.; Roose, B.; Andaji-Garmaroudi, Z.; Orr, K. W. P.; Parker, J. E.; Midgley, P. A.; Dani, K. M.; Stranks, S. D., Local Nanoscale Phase Impurities are Degradation Sites in Halide Perovskites. *Nature* **2022**.
28. Park, J.; Kim, J.; Yun, H. S.; Paik, M. J.; Noh, E.; Mun, H. J.; Kim, M. G.; Shin, T. J.; Seok, S. I., Controlled growth of perovskite layers with volatile alkylammonium chlorides. *Nature* **2023**.
29. Kim, J. S.; Heo, J. M.; Park, G. S.; Woo, S. J.; Cho, C.; Yun, H. J.; Kim, D. H.; Park, J.; Lee, S. C.; Park, S. H.; Yoon, E.; Greenham, N. C.; Lee, T. W., Ultra-bright, efficient and stable perovskite light-emitting diodes. *Nature* **2022,** *611* (7937), 688-694.
30. Fu, Y.; Wu, T.; Wang, J.; Zhai, J.; Shearer, M. J.; Zhao, Y.; Hamers, R. J.; Kan, E.; Deng, K.; Zhu, X. Y.; Jin, S., Stabilization of the Metastable Lead Iodide Perovskite Phase via Surface Functionalization. *Nano Lett* **2017,** *17* (7), 4405-4414.
31. Fu, Y., Stabilization of Metastable Halide Perovskite Lattices in the 2D Limit. *Adv Mater* **2022,** *34* (9), e2108556.
32. Radicchi, E.; Mosconi, E.; Elisei, F.; Nunzi, F.; De Angelis, F., Understanding the Solution Chemistry of Lead Halide Perovskites Precursors. *ACS Appl Energy Mater* **2019,** *2*, 3400-3409.
33. Hamill Jr., J. C.; Schwartz, J.; Loo, Y. L., Influence of Solvent Coordination on Hybrid Organic–Inorganic Perovskite Formation. *ACS Energy Letters* **2018,** *3*, 92-97.
34. Yang, J.; Kim, M.; Lee, S.; Yoon, J. W.; Shome, S.; Bertens, K.; Song, H.; Lim, S.

G.; Oh, J. T.; Bae, S. Y.; Lee, B. R.; Yi, W.; Sargent, E. H.; Choi, H., Solvent Engineering of Colloidal Quantum Dot Inks for Scalable Fabrication of Photovoltaics. *ACS Appl Mater Interfaces* **2021,** *13* (31), 36992-37003.

35. Taylor, A. D.; Sun, Q.; Goetz, K. P.; An, Q.; Schramm, T.; Hofstetter, Y.; Litterst, M.; Paulus, F.; Vaynzof, Y., A general approach to high-efficiency perovskite solar cells by any antisolvent. *Nat Commun* **2021,** *12*, 1878.

36. Fu, W.; Liu, H.; Shi, X.; Zuo, L.; Li, X.; Jen, A. K. Y., Tailoring the Functionality of Organic Spacer Cations for Efficient and Stable Quasi-2D Perovskite Solar Cells. *Adv Funct Mater* **2019,** *29* (25), 1900221.

37. Hui, W.; Chao, L.; Lu, H.; Xia, F.; Wei, Q.; Su, Z.; Niu, T.; Tao, L.; Du, B.; Li, D.; Wang, Y.; Dong, H.; Zuo, S.; Li, B.; Shi, W.; Ran, X.; Li, P.; Zhang, H.; Wu, Z.; Ran, C.; Song, L.; Xing, G.; Gao, X.; Zhang, J.; Xia, Y.; Chen, Y.; Huang, W., Stabilizing black-phase formamidinium perovskite formation at room temperature and high humidity. *Science* **2021,** *371*, 1359-1364.

38. Jeon, N. J.; Noh, J. H.; Kim, Y. C.; Yang, W. S.; Ryu, S.; Seok, S. I., Solvent engineering for high-performance inorganic-organic hybrid perovskite solar cells. *Nature Materials* **2014,** *13* (9), 897-903.

39. Yang, J.; LaFollette, D. K.; Lawrie, B. J.; Ievlev, A. V.; Liu, Y.; Kelley, K. P.; Kalinin, S. V.; Correa-Baena, J. P.; Ahmadi, M., Understanding the Role of Cesium on Chemical Complexity in Methylammonium-Free Metal Halide Perovskites. *Adv Energy Mater* **2022**, 2202880.

40. Fang, H. H.; Yang, J.; Tao, S.; Adjokatse, S.; Kamminga, M. E.; Ye, J.; Blake, G. R.; Even, J.; Loi, M. A., Unravelling Light-Induced Degradation of Layered Perovskite Crystals and Design of Efficient Encapsulation for Improved Photostability. *Adv Funct Mater* **2018,** *28*, 1800305.

41. An, Q. Z.; Paulus, F.; Becker-Koch, D.; Cho, C.; Sun, Q.; Weu, A.; Bitton, S.; Tessler, N.; Vaynzof, Y., Small grains as recombination hot spots in perovskite solar cells. *Matter* **2021,** *4* (5), 1683-1701.

42. Zhang, X.; Munir, R.; Xu, Z.; Liu, Y.; Tsai, H.; Nie, W.; Li, J.; Niu, T.; Smilgies, D. M.; Kanatzidis, M. G.; Mohite, A. D.; Zhao, K.; Amassian, A.; Liu, S. F., Phase Transition Control for High Performance Ruddlesden-Popper Perovskite Solar Cells. *Adv Mater* **2018,** *30* (21), e1707166.

43. Song, H.; Yang, J.; Jeong, W. H.; Lee, J.; Lee, T. H.; Yoon, J. W.; Lee, H.; Ramadan, A. J.; Oliver, R. D. J.; Cho, S. C.; Lim, S. G.; Jang, J. W.; Yu, Z.; Oh, J. T.; Jung, E. D.; Song, M. H.; Park, S. H.; Durrant, J. R.; Snaith, H. J.; Lee, S. U.; Lee, B. R.; Choi, H., A Universal Perovskite Nanocrystal Ink for High-Performance Optoelectronic

Devices. *Adv Mater* **2023,** *35*, 2209486.
44. Zilka, M.; Dudenko, D. V.; Hughes, C. E.; Williams, P. A.; Sturniolo, S.; Franks, W. T.; Pickard, C. J.; Yates, J. R.; Harris, K. D. M.; Brown, S. P., Ab initio random structure searching of organic molecular solids: assessment and validation against experimental data. *Phys Chem Chem Phys* **2017,** *19* (38), 25949-25960.
45. Hu, C.; Shivarudraiah, S. B.; Sung, H. H. Y.; Williams, I. D.; Halpert, J. E.; Yang, S., Discovery of a New Intermediate Enables One-Step Deposition of High-Quality Perovskite Films via Solvent Engineering. *Sol Rrl* **2021,** *5*, 2000712.
46. Soe, C. M. M.; Nie, W. Y.; Stoumpos, C. C.; Tsai, H.; Blancon, J. C.; Liu, F. Z.; Even, J.; Marks, T. J.; Mohite, A. D.; Kanatzidis, M. G., Understanding Film Formation Morphology and Orientation in High Member 2D Ruddlesden-Popper Perovskites for High-Efficiency Solar Cells. *Advanced Energy Materials* **2018,** *8* (1).
47. Giubertoni, G.; Sofronov, O. O.; Bakker, H. J., Effect of intramolecular hydrogen-bond formation on the molecular conformation of amino acids. *Commun Chem* **2020,** *3* (1), 84.
48. Wallace, V. M.; Dhumal, N. R.; Zehentbauer, F. M.; Kim, H. J.; Kiefer, J., Revisiting the Aqueous Solutions of Dimethyl Sulfoxide by Spectroscopy in the Mid- and Near-Infrared: Experiments and Car-Parrinello Simulations. *J Phys Chem B* **2015,** *119* (46), 14780-9.
49. Wang, P.; Chen, X.; Liu, T.; Hou, C. H.; Tian, Y.; Xu, X.; Chen, Z.; Ran, P.; Jiang, T.; Kuan, C. H.; Yan, B.; Yao, J.; Shyue, J. J.; Qiu, J.; Yang, Y. M., Seed-Assisted Growth of Methylammonium-Free Perovskite for Efficient Inverted Perovskite Solar Cells. *Small Methods* **2022,** *6* (5), e2200048.
50. Ma, F.; Li, J.; Li, W.; Lin, N.; Wang, L.; Qiao, J., Stable α/δ phase junction of formamidinium lead iodide perovskites for enhanced near-infrared emission. *Chem Sci* **2017,** *8* (1), 800-805.
51. Xue, J.; Wang, R.; Wang, K. L.; Wang, Z. K.; Yavuz, I.; Wang, Y.; Yang, Y.; Gao, X.; Huang, T.; Nuryyeva, S.; Lee, J. W.; Duan, Y.; Liao, L. S.; Kaner, R.; Yang, Y., Crystalline Liquid-like Behavior: Surface-Induced Secondary Grain Growth of Photovoltaic Perovskite Thin Film. *J Am Chem Soc* **2019,** *141* (35), 13948-13953.